Precision measurements on oxygen formation in stellar helium burning with gamma-ray beams and a Time Projection Chamber

Robin Smith (robin.smith@shu.ac.uk)
Sheffield Hallam University https://orcid.org/0000-0002-9671-8599
Moshe Gai
University of Connecticut
Sarah Stern
University of Connecticut
Deran Schweitzer
University of Connecticut
Mohammad Ahmed
Duke University

Article

Keywords: Time Projection Chamber, Stellar Evolution theory, nuclear reactions

Posted Date: March 10th, 2021

DOI: https://doi.org/10.21203/rs.3.rs-291379/v1

Version of Record: A version of this preprint was published at Nature Communications on October 11th, 2021. See the published version at https://doi.org/10.1038/s41467-021-26179-x.

Precision measurements on oxygen formation in stellar helium burning with gamma-ray beams and a Time Projection Chamber

R. Smith[1,2], M. Gai[2], S. R. Stern[2], D. K. Schweitzer[2], M. W. Ahmed[3,4]
1. Department of Engineering and Mathematics, Sheffield Hallam University, Sheffield, S1 1WB, UK
2. Laboratory for Nuclear Science at Avery Point, University of Connecticut, Groton, CT 06340-6097
3. Triangle Universities Nuclear Laboratory, Duke University, Durham, NC 27708-0308, USA
4. Department of Mathematics and Physics, North Carolina Central University, Durham, NC 27707, USA

Stellar Evolution theory relies on our knowledge of nuclear reactions, with the carbon/oxygen (C/O) ratio, at the end of helium burning, being the single most important input. However, the C/O ratio is still not known with sufficient accuracy, due to large uncertainties in the cross section for the fusion of helium with ^{12}C to form ^{16}O, denoted as the ^{12}C$(\alpha,\gamma)^{16}$O reaction. We present initial results at moderately low energies using a novel method, which is significantly different from the experimental efforts of the past four decades. Precise angular distributions of the ^{12}C$(\alpha,\gamma)^{16}$O reaction were obtained by measuring the inverse ^{16}O$(\gamma,\alpha)^{12}$C reaction with gamma-beams and a Time Projection Chamber detector. These allowed us to measure, for the first time, the interference angle of the $\ell = 1$ and 2 partial waves contributing to this reaction (ϕ_{12}), which agrees with predictions based on the unitarity of the scattering matrix.

NUCLEAR astrophysics, the study of nuclear processes in stars and in the cosmos, is a mature science that, among other topics, led to the theory of stellar evolution. However, in this theory, the uncertainty of the C/O ratio at the end of helium burning still remains significant. In his Nobel speech in 1984, W.A. Fowler stated "*the ratio of ^{12}C to ^{16}O in helium burning is of paramount importance in nuclear astrophysics*" [1], as it still is today. For example, it determines the fate of Type II supernovae (black hole or neutron star) as well as the light curves of Type Ia supernovae, which are used to measure cosmological distances, leading to the recent discovery of the accelerated expansion and Dark Energy.

In stellar helium burning, carbon and oxygen are formed. Since the formation of carbon is rather well understood, the C/O ratio is determined largely by the single remaining uncertain process: the fusion of ^{12}C with an alpha-particle to form ^{16}O, denoted as the ^{12}C$(\alpha,\gamma)^{16}$O reaction. This reaction was successfully measured in terrestrial laboratories to energies below 2 MeV, but it needs to be extrapolated to stellar conditions of a plasma with a temperature of kT ∼20 keV, and the most efficient burning energy of 300 keV (the Gamow window [1]). In stellar conditions two partial waves $\ell = 1$ and 2 contribute, and they are denoted by the spectroscopic $E1$ and $E2$ amplitudes in reaction and scattering theory [1]. The challenges in this field are measurements of angular distributions of the ^{12}C(α,γ) reaction from which the $E1$ and $E2$ cross sections are extracted, for accurate extrapolations to stellar conditions.

Progress was achieved in measuring angular distributions of the ^{12}C(α,γ) reaction by directly measuring the emitted gamma-rays [2–7]. However, large uncertainties remain in the measured E1 and E2 cross sections and their extrapolations to stellar conditions. For example, in a recent analysis by the MIT group [8] of current data, they quote a 100% uncertainty of the extrapolated cross section of the ^{12}C(α,γ) reaction. In contrast, the authors of Ref. [9] concluded that a "level of uncertainty ∼10% may be in sight".

Due to insufficient angular distribution data, previous unconstrained fits using E1 and E2 amplitudes and their mixing phase angle (ϕ_{12}) have hitherto not yielded ϕ_{12} values expected from a theoretical treatment of elastic scattering data [10, 11]: $\phi_{12} = \delta_2 - \delta_1 + \tan^{-1}\eta/2$, where δ_1 and δ_2 are the measured $\alpha + {}^{12}$C elastic scattering phase shifts, and for this system, $\eta = 8 \times \alpha/\beta$, where α is the fine structure constant and $\beta = v/c$. This theoretical prediction is valid in general when the capture cross section is small, and it is the only open reaction channel, as is the case here. It is based on the Watson theorem, which is derived assuming unitarity of the scattering matrix [10, 11]. However, in contrast, the three-parameter angular distribution fits (including ϕ_{12}) of previous measurements, summarised in Table I of [6], do not show agreement between the deduced ϕ_{12} with this most elementary theoretical prediction based on unitarity. The disagreement with a fundamental prediction anchored in quantum mechanics cannot be overlooked.

The modern measurements of gamma-ray data of the ^{12}C(α,γ) reaction [6] were analysed [11, 12], and major uncertainties were concluded. The large uncertainties deduced for the modern data [6] and similar gamma-ray data [13] lead to uncertainties in the R-Matrix analyses and extrapolation to stellar conditions [9]. For example, it was concluded that the centre of mass motion of the $\alpha + {}^{12}$C system leads to large shifts of the centre of mass angles, which were previously ignored [12]. Furthermore, large backgrounds in the measured gamma-ray spectra, induced, for example, by in-beam neutrons (e.g. Fig. 6 of [6]), leads to large uncertainties in the extracted $E1/E2$ cross sections [11]. We conclude that measurements of data with low backgrounds and small corrections are needed for progress in the field.

Results

In this paper, we report a robust extraction of the relative phase ϕ_{12} which agrees with the prediction of unitarity.

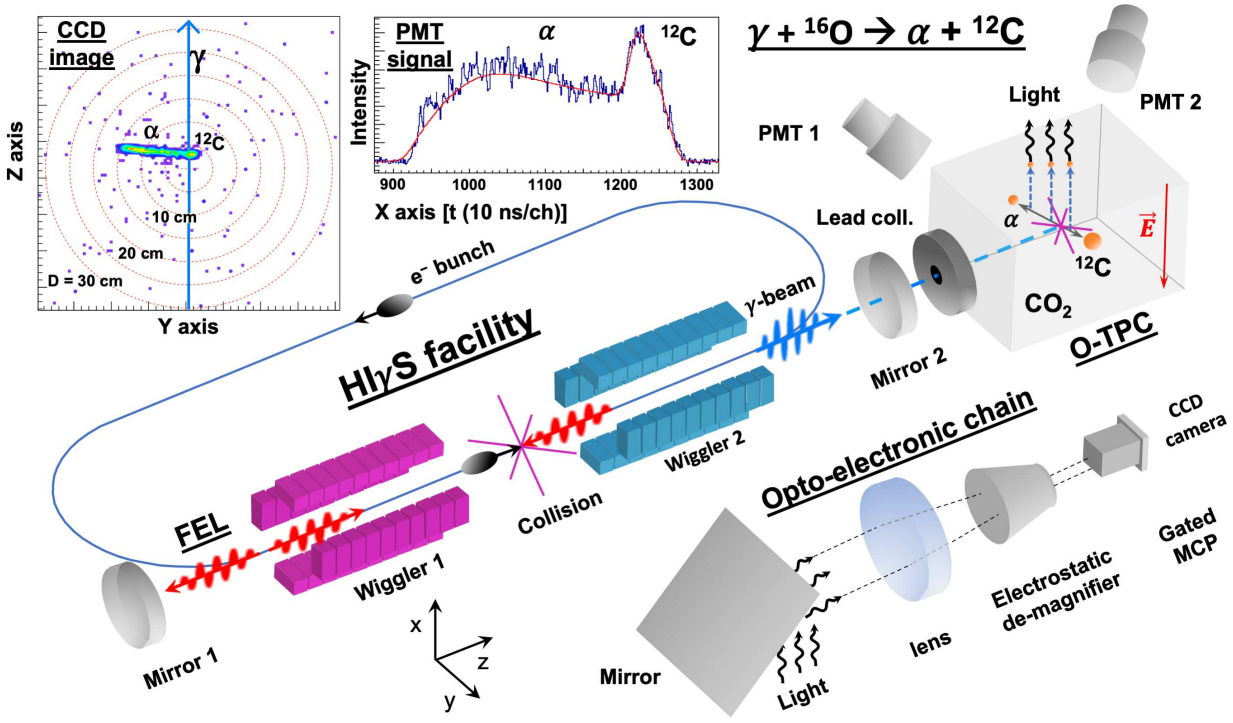

FIG. 1. (Color Online) Schematic diagram of the experimental setup used at the HIγS facility at Duke University, not drawn to scale. The distance between the two mirrors is 53.73 metres, between the FEL-electron collision point and the collimator is 60 metres, and between the collimator and the O-TPC is 20 metres. We show the FEL electron ring, the Compton Backscattered gamma-ray, the O-TPC with the PMTs and the opto-electronic chain, discussed in the text. In the upper left corner we show a typical CCD image of a track and a PMT signal with the fitted line shape of tracks from an α and ^{12}C. The three dimensional track is reconstructed with the (y, z) coordinate measured by the CCD image and the x coordinate calculated using the time projection signal measured by the PMT, as discussed in the text.

We use a novel method that significantly differs from the experimental efforts of the past four decades. Detailed angular distributions of the reaction are measured with an unprecedented $\sim 2^\circ$ resolution, and over almost a full range of polar angles, using a Time Projection Chamber detector with an optical readout (O-TPC). We report on measured $E1 - E2$ mixing phase angles (ϕ_{12}) that are in agreement with the theoretical prediction based on unitarity. We note from the outset that we observe an overall agreement with previous data of our total cross section and an agreement with the general shape of the angular distributions. However, the angular distributions differ slightly in their details.

We concentrate on the measured ϕ_{12} only, as a demonstration of our accurate measurements of angular distributions, and we intend to expand in future publications our extracted E1 and E2 cross sections. Our initial success in measuring precise angular distributions, reported here, encourages us to extend our measurements to lower energies, using a TPC detector [14] and gamma-ray beams from the HIγS facility [15, 16] in the USA and the newly constructed ELI-NP facility [17, 18] of the EU.

Inverse process (detailed balance). In our experiment, instead of measuring the fusion of $\alpha + {}^{12}$C to form ^{16}O, we use gamma-ray beams, to measure the time reversed process: the $^{16}\mathrm{O}(\gamma,\alpha)^{12}\mathrm{C}$ photo-dissociation reaction. The photo-dissociation cross section is directly related to the capture cross section via the principle of detailed balance − see equation 9 of [17] − and is larger by a factor of ∼50. This process does not require significant centre of mass corrections. More importantly, we measure the tracks of the emanating α and ^{12}C in a Time Projection Chamber (TPC) detector operating with CO_2 gas [19]. The ^{16}O photo-dissociation events are unambiguously identified and measured in a $\sim 4\pi$ geometry with high efficiency, and a vanishingly small background, as shown in Fig. 1. Since the angular distributions are measured in a single detector, the relative corrections between different angles (which are essential for measurements with a gamma detector array) are negligible. These factors allow us to measure angular distributions of the $^{12}\mathrm{C}(\alpha,\gamma)$ reaction with high precision, as we report here.

Gamma beam. Intense, quasi mono-energetic photon beams were produced at the High Intensity γamma Source (HIγS) of the Triangle Universities Nuclear Laboratory, as discussed in Ref. [15]. Briefly, as depicted in Fig. 1, high energy gamma beams were generated through the inverse-Compton scattering of an electron bunch with the free-electron-laser (FEL) pho-

tons, produced by the previous electron bunch [15]. The gamma beam energy is determined by the FEL wavelength and the electron energy. A circularly polarised gamma beam was used in order to limit the wear of optical components. Data were taken using beam intensities of $\sim 10^8 \gamma$/s with an energy spread of $\sim$3%, at the following nominal beam energies: E_γ = 9.08, 9.38, 9.58, 9.78, 10.1, and 10.4 MeV.

The gamma beam was defined by a 15cm-long lead collimator with an 11mm-diameter aperture. It then passed successively through five thin scintillating paddles that were used for on-line measurements of the beam flux. The gamma beam then passed through air to reach a 5μm kapton window, which isolated the gas in the O-TPC from atmosphere. This was followed by a strong permanent magnet, which deflected electrons produced in the window away from the gaseous target.

Downstream of the O-TPC, the flux was also measured by detecting neutrons from the $d(\gamma, n)p$ reaction using an in-beam D_2O target. Prior to each measurement, copper of various thicknesses were inserted to attenuate the beam by up to a factor of 10^5. The remaining photons were incident on an HPGe or NaI(Tl) detector, to measure the photon energy and flux, respectively. The 10-inch NaI(Tl) detector provided the absolute number of photons in the attenuated beam, which was used to cross-calibrate the relative flux paddle detectors. The energy of beam was obtained using a large, high-efficiency HPGe detector. The measured spectra were unfolded using a Monte Carlo technique [20–22] to obtain the energy profile of the beam. The O-TPC detector was aligned with respect to the beam using a gamma camera and lead absorbers placed in the front and back of the detector as discussed in [20, 21].

The O-TPC detector. The detector operation is discussed in Ref. [19]. Briefly, it was operated with a gas mixture of CO_2 (80%) and N_2 (20%), at 100 Torr pressure. The active gas volume was 30×30×21 cm^3. The 12mm-wide gamma beam entered the active volume through a 15mm opening. The N_2 gas was used to produce the near-UV (338 nm) light detected by the PMTs and the opto-electronic chain. The resulting α and ^{12}C from the photo-dissociation of ^{16}O propagated through the gas and ionised atoms along their tracks, with an energy loss profile that was calculated using SRIM [23], giving the line-shape shown in Fig. 1. The electrons drift upwards in the O-TPC under the influence of a $\sim$ 200 V/cm electric field (2 V/cmTorr reduced electric field). The drift velocity of the electrons was measured to be 11.1 mm/μs, in agreement with calculations using Magboltz [24].

The drift electrons were then multiplied by a stronger electric field of 20 V/cmTorr, giving rise to an avalanche and producing light. The light was detected by four photomultiplier tubes (PMTs) that surrounded the top of the O-TPC, as depicted in Fig. 1. The PMT signals were digitised with a 100 MHz 12-bit flash ADC. The PMT signals measure the arrival times of the drift electrons, recording the *time projection* of the track, which allows us to measure the x-coordinate, as shown in Fig. 1. At the same time, optical photons propagate through the opto-electronic chain and are focussed onto a CCD camera, which photographs the track. An image of a typical track from the $^{16}O(\gamma,\alpha)^{12}C$ reaction is shown as the left figure in Fig. 1. The photograph allows us to measure the y-z coordinates of the track. The combination of the time projection (x) and CCD image (y,z) provides the 3-dimensional coordinates of the track, from which the scattering angles were determined.

The anode signal, track length, and the total light signal were used to measure the total energy deposited, event-by-event, in the TPC. Tracks in the O-TPC were calibrated using the 3.183 MeV α particles from a standard ^{148}Gd radioactive source. The energy resolution was measured to be 4% (FWHM). The particle identification was achieved by measuring dE/dx of the particles along the track. These line-shapes were used to determine the photo-dissociation events, as shown in Fig. 1.

Background. Events recorded by the O-TPC include: Compton electrons, cosmic rays, $^{14}N(\gamma,p)$, $^{16,18}O(\gamma,\alpha)$, and $^{12}C(\gamma,\alpha)^8$Be reactions. Compton electrons deposit up to 100 keV total energy in the O-TPC, and were removed by an 800 keV electronics threshold on the anode signal. The majority of the cosmic events were removed by inspecting the track image and requiring an interaction point which is within ±6 mm of the centre of the gamma-beam position. Events from the $^{14}N(\gamma,p)$ reaction were removed by identifying the dE/dx line-shape of the proton, which differs significantly from the α particles. The $^{18}O(\gamma,\alpha)$ reaction events deposit 934.95 keV more energy than the $^{16}O(\gamma,\alpha)$ events, and were easily removed by measuring the total energy deposited in the O-TPC. However, the energy deposited by the ^{12}C dissociation events is only 112.85 keV lower than for ^{16}O dissociation events. Hence, the ^{12}C dissociation events could not be removed by relying solely on the total energy deposited in the O-TPC, which was measured with $\sim$100 keV resolution.

Line-shape analysis. The analysis of the $^{12}C(\gamma,\alpha)$ events was already reported [25, 26]. Namely, the measured PMT line-shape was fitted with the line-shapes predicted for ^{12}C and ^{16}O dissociation events, and the resulting reduced χ^2/ν of each best fit was derived. In Fig. 2, we show a two-dimensional lego plot of the obtained reduced χ^2/ν, demonstrating a clear separation of the ^{12}C and ^{16}O dissociation events with small background. This was followed by a visual inspection of the remaining events to remove the small number of background events.

The reconstructed three dimensional track allowed us to measure the scattering angle and azimuthal angle of each event. The CCD image measured the in-plane angle (α), and the PMT signal the out of plane angle (β), from which the scattering angle (θ) and azimuthal angle (ϕ) were calculated [19]: $\tan\phi = \tan\beta/\sin\alpha$ and $\cos\theta = \cos\beta \times \cos\alpha$.

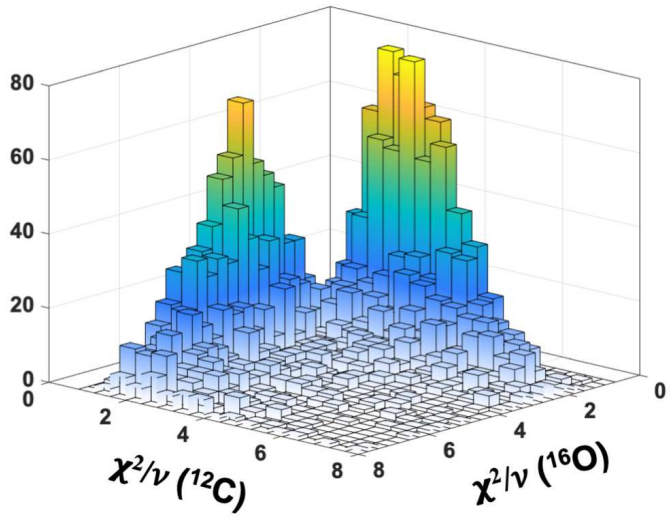

FIG. 2. (Color Online) Two dimensional Lego plot of smallest deduced χ^2/ν of fitting the PMT line-shape with the predicted line shapes of ^{16}O and ^{12}C dissociation events.

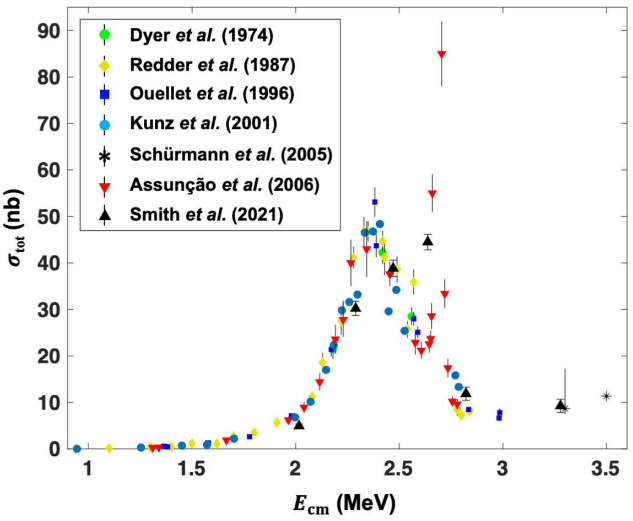

FIG. 3. (Color Online) The total reaction cross section measured in this work, with a gamma beam resolution of $\sigma \sim$120 keV, compared with previous measurements using particle beams, with considerably better energy resolutions. The average of the shown previous world data was used to calculate the "effective energy" of our measurement with a broad gamma-beam.

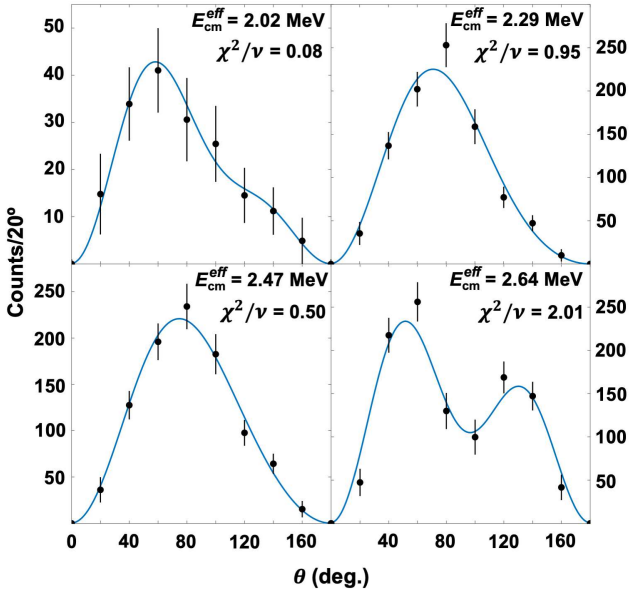

FIG. 4. (Color Online) The measured angular distributions (including efficiency corrections) at the shown "effective" centre of mass energies, with the three parameter fit ($|A_{E1}|$, $|A_{E2}|$, and ϕ_{12}) of the partial wave decomposition.

The efficiency for detecting ^{16}O(γ,α) events was calculated using Monte Carlo simulations. We define the fiducial volume over $|\beta| < 55°$ to exclude the region where the scattering angle carries the largest uncertainty. Over the selected fiducial volume, we obtained an angular resolution better than 2°. The fiducial volume was further restricted to $|\beta| > 20°$ in order to provide the cleanest separation of ^{16}O and ^{12}C dissociation events. The Monte Carlo simulation also accounted for edge effects, where one of the particles escapes the detector, meaning that only a section of the track is contained inside the fiducial volume. The efficiency rises from 0% to 60% for scattering angles, θ, between 20° and 55°. The efficiency varies between 60% and 40% between 55° and 90°.

Measured Cross Sections. For each nominal beam energy E_γ = 9.38, 9.58 and 9.78 MeV, we accumulated ∼500 ^{16}O photo-dissociation events. For E_γ = 9.08, 10.1 and 10.4 MeV, we accumulated ∼100 events. The actual gamma beam energies were measured using the attenuated beam and HPGe detector. The measured beam energies, with 30 keV uncertainties, were: E_γ(HPGe) = 9.01, 9.41, 9.61, 9.78, 10.10, and 10.43 MeV. The average of the previous world data (plotted in Fig. 3) was used to calculate the "effective energies" of our measurements over the FWHM of the broad gamma-beam. These are: E_γ^{eff} = 9.18, 9.45, 9.63, 9.80, 9.98 and 10.44 MeV corresponding to effective centre-of-mass energies $E_{c.m.}^{eff}$ = 2.02, 2.29, 2.47, 2.64, 2.82, and 3.28 MeV. The integrated total beam intensity was measured using the plastic paddle detectors, which were calibrated to absolute flux using the attenuated beam and 10" NaI(Tl) detector. There is an estimated 11% uncertainty in the beam flux, due to uncertainties in the copper attenuators. The counts at each beam energy, along with the beam flux and the efficiency, were used to calculate the total cross section of the ^{16}O(γ,α) reaction, from which we derived the cross section of the ^{12}C(α,γ) reaction, as shown in Fig. 3, using detailed balance (equation 9 of [17]). These show only statistical error bars, excluding the global 11% systematic uncertainty. An overall agreement with previous data is observed, emphasising

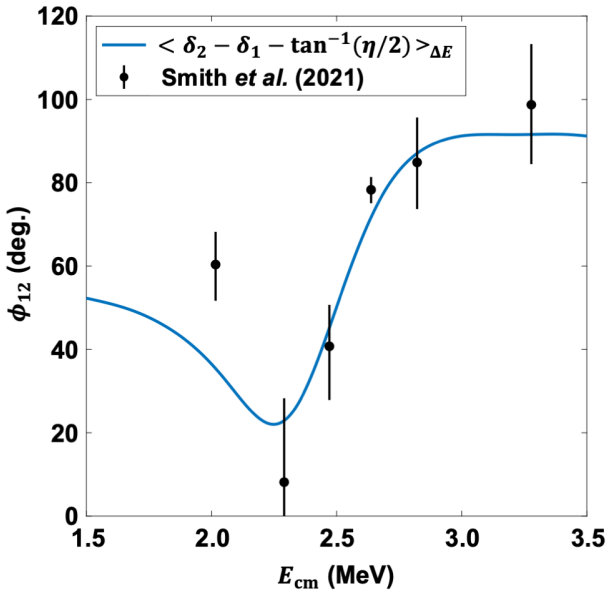

FIG. 5. (Color Online) The measured E1-E2 mixing phase angle (ϕ_{12}), compared to the phase angle predicted by unitarity, convolved with the gamma beam energy resolution of $\sigma \sim 120$ keV, shown as the solid line.

the applicability of our method.

Fitted Angular Distributions. The scattering angle in the laboratory frame was converted to the centre-of-mass scattering angle (shift $< 2°$). Measured events were separated into 20° angular bins and efficiency corrections were applied to each angular bin. The obtained angular distributions are shown in Fig. 4. They were fitted with the partial wave decomposition [2]

$$\begin{aligned} W(\theta) = &(3|A_{E1}|^2 + 5|A_{E2}|^2)P_0(\cos\theta) \\ &+ \left(^{25}/_{7}|A_{E2}|^2 - 3|A_{E1}|^2\right) P_2(\cos\theta) \\ &- {}^{60}/_{7}|A_{E2}|^2 P_4(\cos\theta) \\ &+ 6\sqrt{3}|A_{E1}||A_{E2}|\cos\phi_{12}\left[P_1(\cos\theta) - P_3(\cos\theta)\right], \end{aligned}$$

by varying all three fit parameters: A_{E1}, A_{E2} and ϕ_{12}. The theoretical angular distributions were convolved with a Gaussian to account for a 2° angular uncertainty and were averaged over the 20° bin widths. The obtained χ^2/ν fit values are 0.08, 0.95, 0.50, 2.01, 0.41, and 0.61 at $E^{eff}_{c.m.}$ = 2.02, 2.29, 2.47, 2.64, 2.82, and 3.28 MeV, respectively. The low statistics (a factor of ∼5 smaller) of the angular distribution measured at 2.02 MeV lead to a non statistical ensemble of data points, and the resulting fit is over-determined. However, we still use the usual statistical procedure (minimum $\chi^2 + 1$) to quote the uncertainties of the extracted fit parameters.

Discussion

The obtained E1−E2 mixing phase angles (ϕ_{12}) are shown in Fig. 5. The theoretically predicted ϕ_{12}, discussed above, averaged over the beam energy resolution (FWHM = 300 keV), is also plotted in Fig. 5. Our measured ϕ_{12} values are found to be in agreement with the theoretical prediction down to $E^{eff}_{c.m.} = 2.29$ MeV, and exhibit the correct trend below this energy. We note that for the lowest energy angular distribution, we obtained 83 raw counts − not enough to obtain a statistically significant result. However, at this stage, we have demonstrated the applicability of our new experimental method, and we intend to embark on a longer experimental campaign to remeasure these data and probe lower energies. Most importantly, we observe for the first time the predicted dip at 2.4 MeV, unlike previous measurements [6].

In conclusion, we have presented a measurement of the $^{12}C(\alpha,\gamma)^{16}O$ reaction, using an entirely different approach to previous experimental efforts. Our method permitted us to measure angular distributions with high precision and, for the first time, we deduce the E1−E2 mixing phase (ϕ_{12}), which is in agreement with the prediction of fundamental theory based on unitarity of the scattering matrix. This demonstrates the power of our experimental approach as a promising new tool to investigate the cross section of the $^{12}C(\alpha,\gamma)^{16}O$ reaction at gamma beam facilities.

Methods

The O-TPC allows us to reconstruct, in three dimensions, the events corresponding to the $^{16}O(\gamma,\alpha)^{12}C$ reaction, by measuring all information pertaining to the reaction [19]. It measures the total energy deposited, the particle type, momentum, and angular distributions of the emitted particles. Thus, it allowed us to differentiate different reactions using three main tools: the photograph taken by the CCD camera, the total energy deposited by each event, and the time projection of each track. Further details of the analysis methods are provided below.

Image processing. At the beginning of each run, a photograph of the TPC was taken without the incident beam, which was subtracted from each image of a track. An example $^{12}C + \alpha$ track (zoomed), after this correction, is shown in Fig. 6 a). The average background pixel value, $\bar{p}$, and its standard deviation, σ_p, were quantified, and a threshold of $\bar{p} + 5\sigma_p$ applied. All pixel values below this threshold were set to zero. This results in Fig. 6 a1). The resolution of the image was then degraded by a factor of 4 in each direction, resulting in Fig. 6 a2). The *hot* pixels surrounding the main track correspond to partial tracks of electrons that scatter during the ionisation. These are removed by zeroing the pixel values in the compressed image that do not have 5 or more non-zero neighbouring pixels. This gives Fig. 6 a3). Finally, with a mask provided by the remaining non-zero pixels, the original resolution of the image was restored to give Fig. 6 a4).

For highly ionising $^{12}C + \alpha$ and $^{14}C + \alpha$ tracks, corresponding to photo-dissociation of ^{16}O and ^{18}O, respectively, the final image consists of a single cluster of non-zero pixels on a blank background. Sparks in the TPC

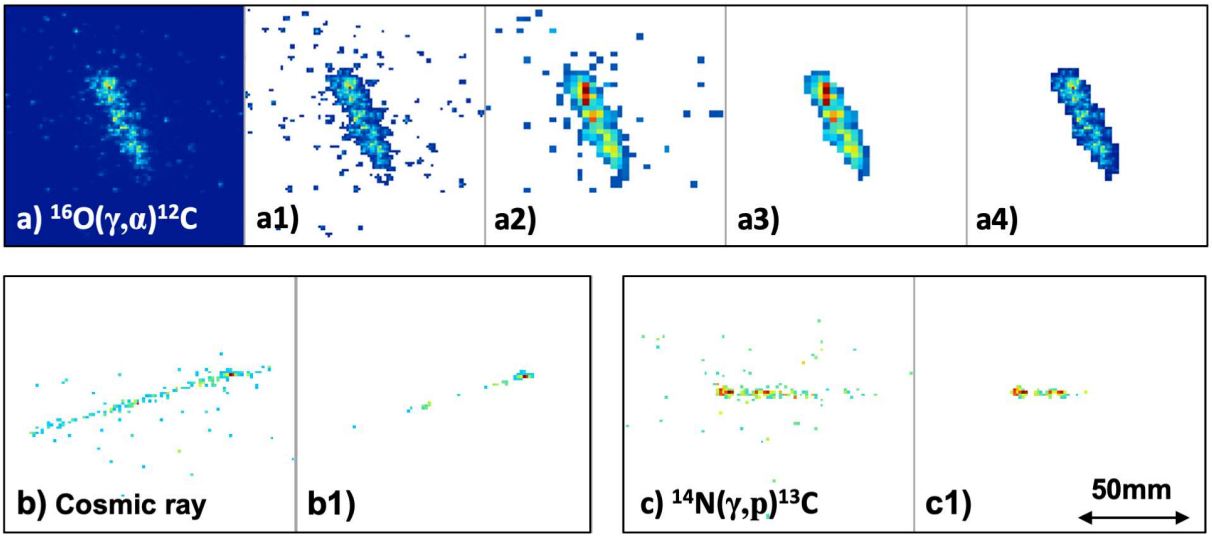

FIG. 6. (Color Online) Image processing steps for the photo-dissociation and cosmic events: a) $^{16}\mathrm{O}(\gamma,\alpha)^{12}\mathrm{C}$, b) cosmic ray, c) $^{14}\mathrm{N}(\gamma,p)^{13}\mathrm{C}$.

generate large numbers of clusters and are readily removed. Proton tracks induced by cosmic rays and from the photo-dissociation of ^{14}N, shown in Figs. 6 b) and Fig. 6 c), respectively, result in two or more clusters of non-zero pixels. This is because the stopping power of the proton is much lower than the $^{12/14}\mathrm{C}+\alpha$. This leads to low pixel values, closer to the background level. Only tracks with ≤ 2 clusters of pixels were taken for further analysis. A second data reduction cut was placed, demanding that the origin of each track lay within ±6mm of the beam position. These two data analysis cuts removed ∼70% of raw events.

From each image, the angle of the track in the y-z plane, relative to the beam direction, α, was extracted. The y-z coordinates of each pixel in a track were plotted and a linear fit was performed. The fit was weighted by the each pixel's intensity. The error on the gradient was extracted using standard techniques, which led to a typical uncertainty on the extracted α angle of ∼2°.

Track length and energy deposition. For each event, the two pixels with the largest separation were used to deduce the length of the track in the y-z plane of the coordinate system shown in Fig. 1. The x length was extracted from the time projection. These were combined to obtain the total track length. Additionally, the energy deposited by each event in the TPC was measured using the total pulse height. As expected, the track length and energy were correlated. A 2D plot of track length vs. energy is shown in Fig. 7. Regions of high intensity in this plot correspond to different reactions. With similar Q-values, the ^{12}C and ^{16}O photo-dissociation events appear within the same peak. The ^{18}O photo-dissociation Q-value differs sufficiently (935 keV) that these events appear as a separate peak. A 2D software cut was placed around the $^{12}\mathrm{C}/^{16}\mathrm{O}$ peak to remove all other types of events.

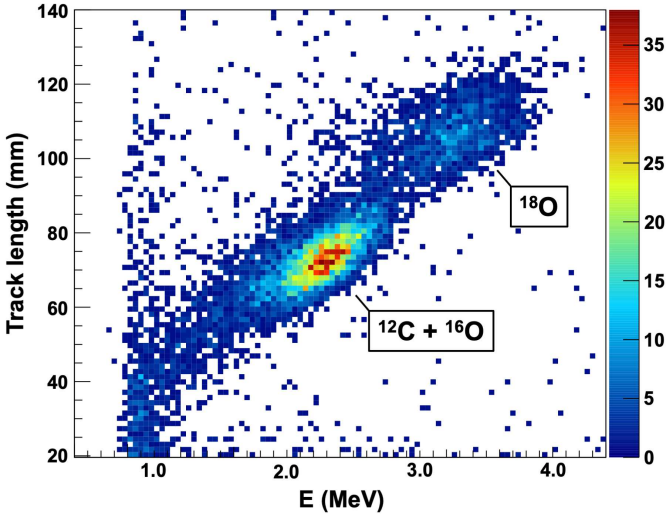

FIG. 7. (Color Online) Histogram of track length vs. deposited energy.

Lineshape analysis. In order to differentiate between the remaining $^{12}\mathrm{C}/^{16}\mathrm{O}$ events, and to extract the out-of-plane angle, β, a lineshape analysis was performed. The shape of the time projection depends on the stopping powers of the reaction products along with the β angle of the track. Tracks with large β result in long time projections, and those with small β give short time projections, corresponding to the track lengths in the x-direction. The SRIM software [23] was used to determine lineshapes for each type of photo-dissociation event: $^{16}\mathrm{O}\rightarrow{}^{12}\mathrm{C}+\alpha$ and $^{12}\mathrm{C}\rightarrow 3\alpha$. These were then pro-

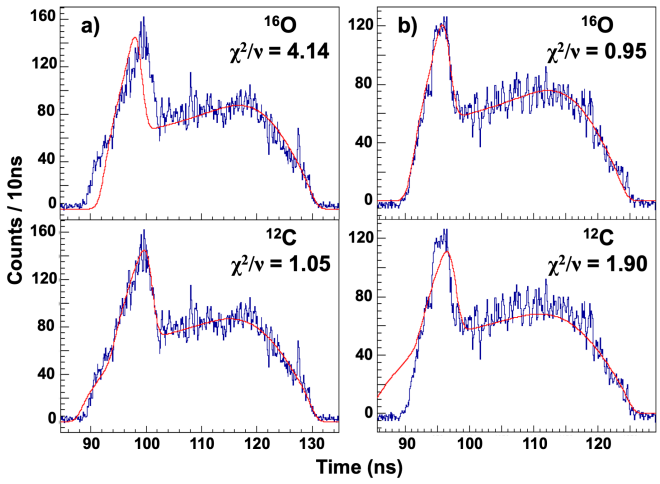

FIG. 8. (Color Online) Example lineshape fits used to distinguish ^{12}C/^{16}O events. a) A typical ^{12}C photo-dissociation time projection. b) A typical ^{16}O photo-dissociation time projection. The upper and lower panels show the best fits of ^{16}O and ^{12}C photo-dissociation theoretical lineshapes, respectively.

jected for β angles ranging between $\pm 90°$. Each of the 180 β projections for both ^{12}C and ^{16}O were fitted to the time projection of each event. The β angle of the event was obtained through a χ^2 minimisation. Differentiating between ^{12}C and ^{16}O events was achieved by examining the relative χ^2/ν of the $^{16}\mathrm{O} \rightarrow {}^{12}\mathrm{C} + \alpha$ and $^{12}\mathrm{C} \rightarrow 3\alpha$ best fits, as shown in Fig. 8. A histogram of the relative χ^2/ν values was shown earlier in Fig. 2. A diagonal software cut through the centre of Fig. 2 removed the majority of ^{12}C events from the data, preserving, on average, 95% of ^{16}O events.

Visual inspection. All remaining events underwent a visual inspection, to remove the small number of ^{12}C events that escaped earlier software cuts. Along with the time projection, the lateral projection of the image of each track was also fitted with the $^{16}\mathrm{O} \rightarrow {}^{12}\mathrm{C} + \alpha$ lineshape projected into the y-z plane, which provided a further dimension for event rejection.

Data and code availability. The lead author would like to acknowledge the efforts of the TUNL-OTPC collaboration for the collection and dissemination of data and support of the Department of Energy under grant number DE-FG02-97ER41033. The data have been made publicly available for re-analysis under a Creative Commons BY-NC 4.0 licence. The image files of tracks on an event-by-event basis, the root files containing the time projections and energy signals, the root files containing the beam intensity monitoring data, along with example analysis codes, are available on the Sheffield Hallam University data repository at: `www.shu.ac.uk/____/`

[1] W. A. Fowler, Rev. Mod. Phys. **56**, 149 (1984).
[2] P. Dyer and C. A. Barnes, Nuc. Phys. **A233**, 495 (1974).
[3] A. Redder, *et al.*, Nuc. Phys. **A462**, 385 (1987).
[4] J. M. L. Ouellet, *et al.*, Phys. Rev. C **54**, 4 (1996).
[5] R. Kunz, *et al.*, Phys. Rev. Lett **86**, 15 (2001).
[6] M. Assuncao *et al.*, Phys. Rev. C **73**, 055801 (2006).
[7] D. Schuermann, *et al.*, Phys. Lett. B **703**, 557 (2011).
[8] I. Friscic, T. W. Donnelly, and R. G. Milner, Phy. Rev. C **100**, 025804 (2019).
[9] R. J. DeBoer, J. Goerres, M. Wiescher, R. E. Azuma, A. Best, C. R. Brune, C. E. Fields, S. Jones, M. Pignatari, D. Sayre, K. Smith, F. X. Timmes and E. Uberseder, Rev. Mod. Phys. **89**, 035007 (2017).
[10] C. R. Brune, Phys. Rev. C **64**, 055803 (2001).
[11] Moshe Gai, Phys. Rev. C **88**, 062801(R) (2013).
[12] C. R. Brune and D. B. Sayre; Nucl. Instr. Meth. A **698**, 49 (2013).
[13] Michael Fey, Ph.D. thesis, Universitaet Stuttgart, 2004, DOI:10.18419/OPUS-4716 Corpus ID: 94353597.
[14] M. Gai , D. Schweitzer, S. R. Stern, A. H. Young, R. Smith, M. Cwiok, J. S. Bihalowicz, H. Czyrkowski, R. Dabrowski, W. Dominik, A. Fijalkowska, Z. Janas, L. Janiak, A. Korgul, T. Matulewicz, C. Mazzocchi, M. Pfuetzner, M. Zaremba, D. Balabanski, I. Gheorge, C. Matei, O. Tesilenau, V. N. Zamfir, M. W. Ahmed, S. S. Henshaw, C. R. Howell, J. M. Mueller, L. S. Myers, S. Stave, C. Sun, H. R. Weller, Y. K. Wu, A. Breskin, V. Dangendorf, K. Tittelmeier, Nucl. Instr. Meth. **A954**, 161770 (2020).
[15] Henry R. Weller, Mohammad W. Ahmed, Haiyan Gao, Werner Tornow, Ying Wu, Moshe Gai, Rory Miskimen, Prog. Part. Nucl. Phys. **62**, 257 (2009).
[16] HIγS Approved Proposal P-18-19, Moshe Gai (co-Spokesperson), Deran K. Schweitzer, Sarah R. Stern, Wojciech Dominik (co-Spokesperson), Mikolaj Cwiok, Aleksandra Fijalkowska, Mateusz Fila, Amanda Giska, Agnieszka Korgul, Zenon Janas, Tomasz Matulewicz, Robin Smith, Dimiter L. Balabanski, Dario Lattuada, and Catalin Matei.
[17] D. Filipescu, A. Anzalone, D. L. Balabanski, S. S. Belyshev, F. Camera, M. La Cognata, P. Constantin, L. Csige, P. V. Cuong, M. Cwiok, V. Derya, W. Dominik, M. Gai, S. Gales, I. Gheorghe, B.S. Ishkhanov, A. Krasznahorkay, A. A. Kuznetsov, C. Mazzocchi, V. N. Orlin, N. Pietralla, M. Sin, K.A. Stopani, O. Tesileanu, C. A. Ur, I. Ursu, H. Utsunomiya, V. V. Varlamov, H. R. Weller, N. V. Zamfir, and A. Zilges, Eur. Phys. J. A bf 51, 185 (2015).
[18] ELI-NP, Letter of Intent, February 13, 2020, Wojciech Dominik (co-Spokesperson), Mikolaj Cwiok, Aleksandra Fija kowska, Mateusz Fila, Artur, Kalinowski, Agnieszka Korgul, Zenon Janas, Tomasz Matulewicz, Chiara Mazzocchi, Marek Pfuetzner, Marcin Zaremba, Moshe Gai (co-Spokesperson), Deran K. Schweitzer, Sarah R. Stern (LNS at Avery Point, Dimiter L. Balabanski, Sohichiroh Aogaki, Catalin Matei, and Teodora Petruse, Robin Smith, Martin Freer, Tzany Kokalova and Carl Wheldon.
[19] M. Gai, M.W. Ahmed, S.C. Stave, W.R. Zimmerman, A. Breskin, B. Bromberger, R. Chechik, V. Dangendorf,

Th. Delbar, R.H. France III, S.S. Henshaw, T.J. Kading, P.P. Martel, J.E.R. McDonald P.-N. Seo, K. Tittelmeier, H.R. Weller and A.H. Young, JINST **5**, 12004 (2010).
[20] C. Sun and Y. K. Wu; Phys. Rev. ST Accel. Beams **14**, 044701 (2011).
[21] C. Sun, Y. Wu, G. Rusev, and A. Tonchev; Nucl. Inst. Meth. Phys. Res., A **605**, 312 (2009).
[22] C. Sun; Ph.D. thesis, Duke University, 2010, https://dukespace.lib.duke.edu/dspace/bitstream/handle/10161/1579/D_Sun_Changchun_a_200912.pdf?sequence=1
[23] J.F. Ziegler, "The Stopping and Range of Ions in Matter", SRIM 2013, http://www.srim.org.
[24] Stephen Biagi, "Magboltz-transport of electrons in gas mixtures", https://magboltz.web.cern.ch/magboltz/.
[25] W. R. Zimmerman, M.W. Ahmed, B. Bromberger, S. C. Stave, A. Breskin, V. Dangendorf, Th. Delbar, M. Gai, S. S. Henshaw, J. M. Mueller, C. Sun, K. Tittelmeier, H. R. Weller, and Y. K. Wu, Phys. Rev. Lett. **110**, 152502 (2013).
[26] R. Smith, M. Gai, M. W. Ahmed, M. Freer, H. O. U. Fynbo, D. Schweitzer, and S. R. Stern, Phys. Rev. C **101**, 021302(R) (2020).

Acknowledgements The lead author would like to acknowledge the efforts of the UConn-TUNL collaboration for the collection and dissemination of data. The authors would like to thank the staff of HIγS at Triangle Universities Nuclear Laboratory for the operation of the facility, and C. R. Howell for in-depth discussions and assistance with various aspects of the work.

Author contributions M. Gai served as the spokesperson of the UConn-TUNL collaboration [19, 25]. M. Ahmed assisted in data collection. The data were subsequently analysed by R. Smith with the assistance of S.R. Stern and D.K. Schweitzer. All authors contributed to the final manuscript.

Funding This material is based on work supported by the U.S. Department of Energy, Office of Science, Office of Nuclear Physics grants DE-FG02-94ER40870, DE-SC0005367, DE-FG02-97ER41033 and DE-FG02-91ER-40608.

Competing Interests The authors declare that they have no competing financial interests.

Correspondence Correspondence and requests for materials should be addressed to R.S. (email: robin.smith@shu.ac.uk).

Figures

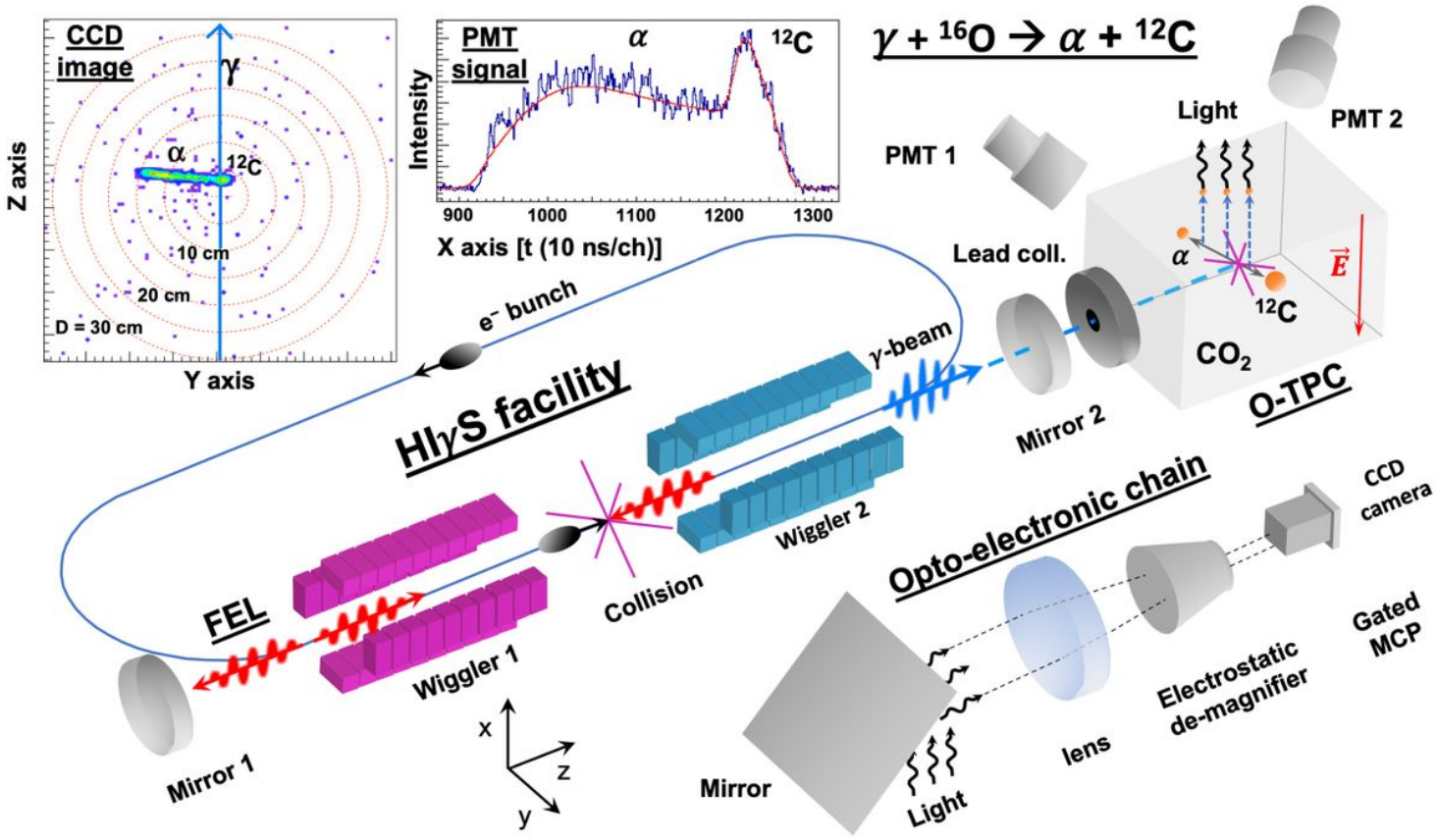

Figure 1

Schematic diagram of the experimental setup used at the HI S facility at Duke University, not drawn to scale. The distance between the two mirrors is 53.73 metres, between the FEL-electron collision point and the collimator is 60 metres, and between the collimator and the O-TPC is 20 metres. We show the FEL electron ring, the Compton Backscattered gamma-ray, the O-TPC with the PMTs and the opto-electronic chain, discussed in the text. In the upper left corner we show a typical CCD image of a track and a PMT signal with the fitted line shape of tracks from an a and 12C. The three dimensional track is reconstructed with the (y; z) coordinate measured by the CCD image and the x coordinate calculated using the time projection signal measured by the PMT, as discussed in the text.

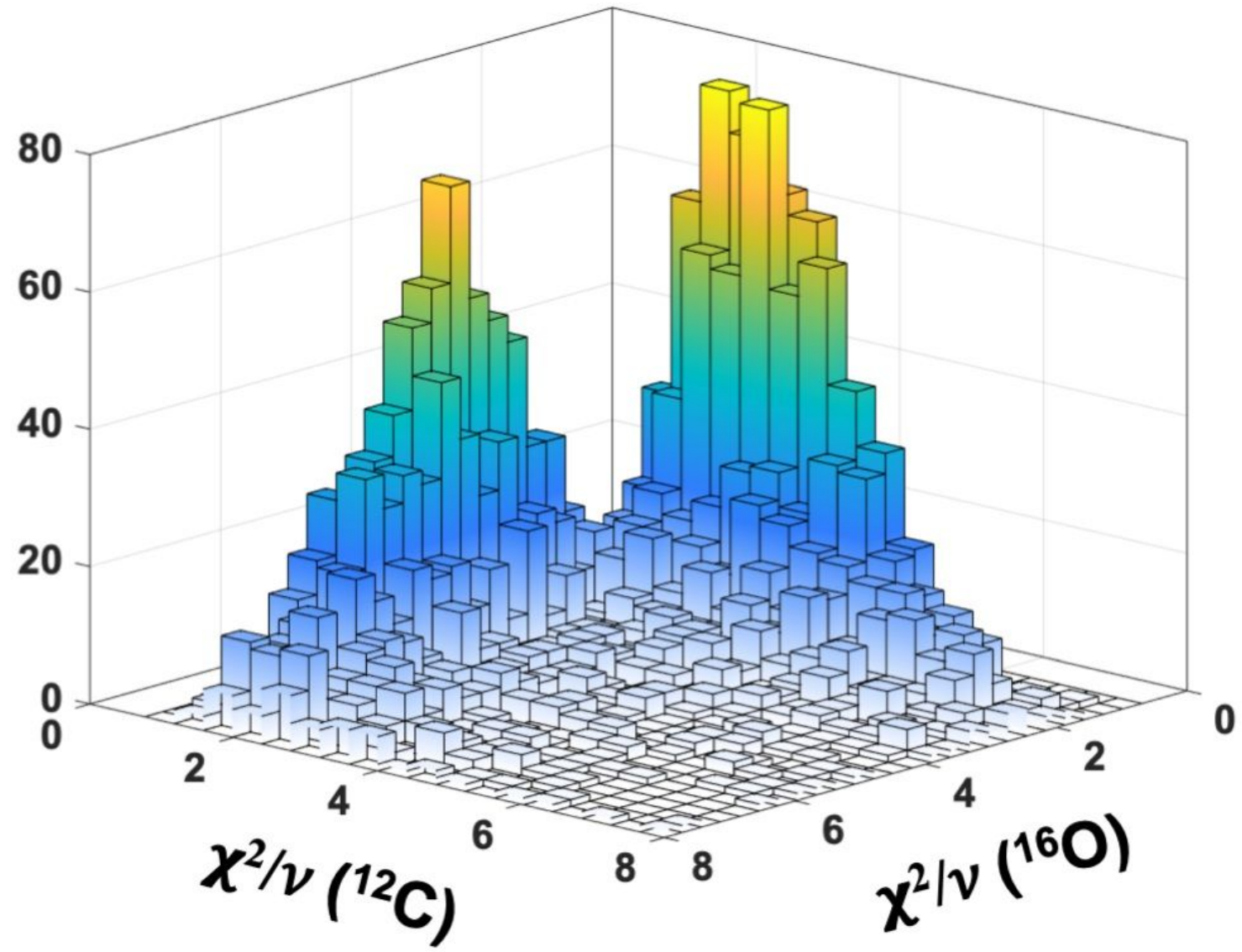

Figure 2

Two dimensional Lego plot of smallest deduced x2=v of fitting the PMT line-shape with the predicted line shapes of 16O and 12C dissociation events.

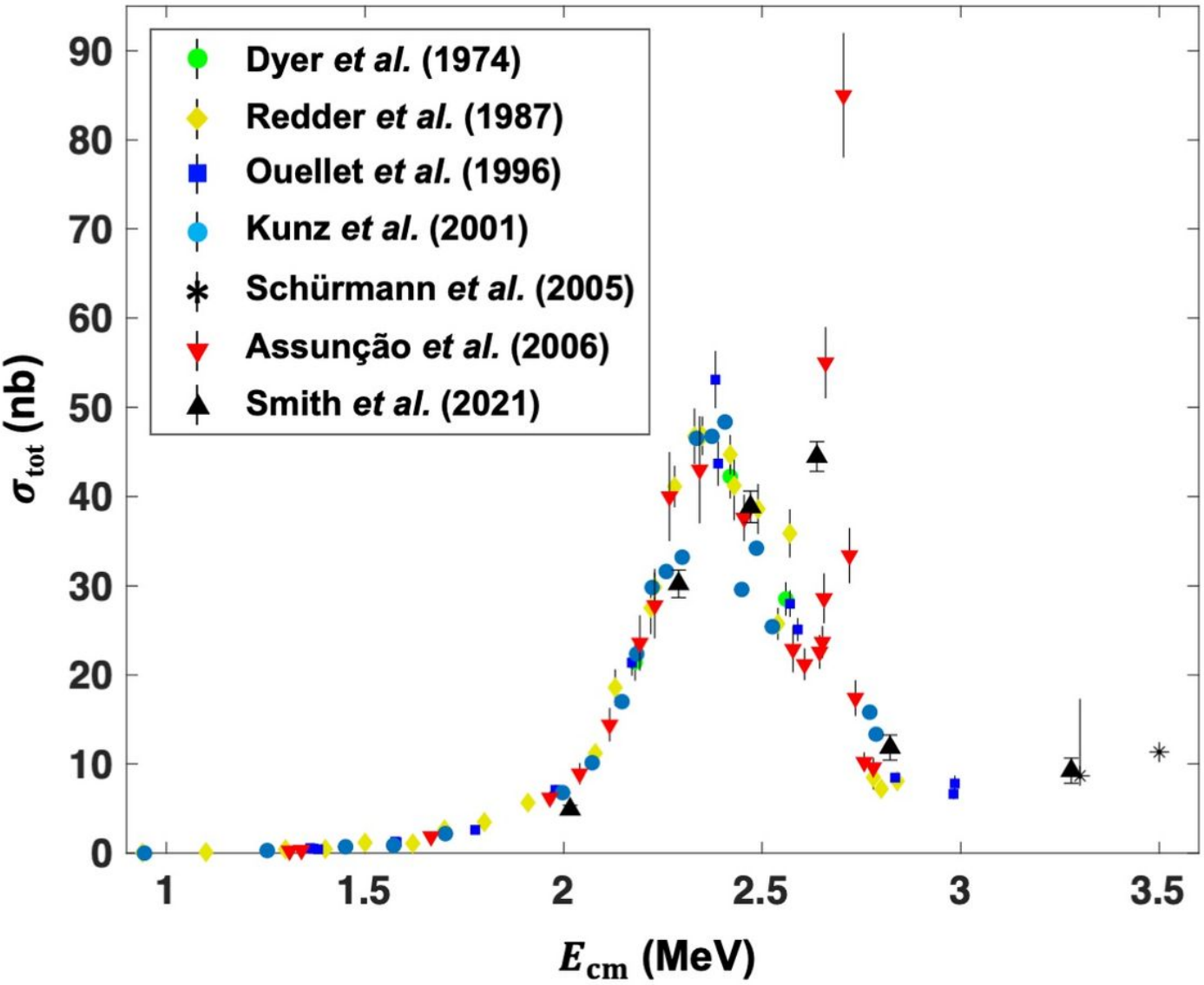

Figure 3

The total reaction cross section measured in this work, with a gamma beam resolution of 120 keV, compared with previous measurements using particle beams, with considerably better energy resolutions. The average of the shown previous world data was used to calculate the "effective energy" of our measurement with a broad gamma-beam.

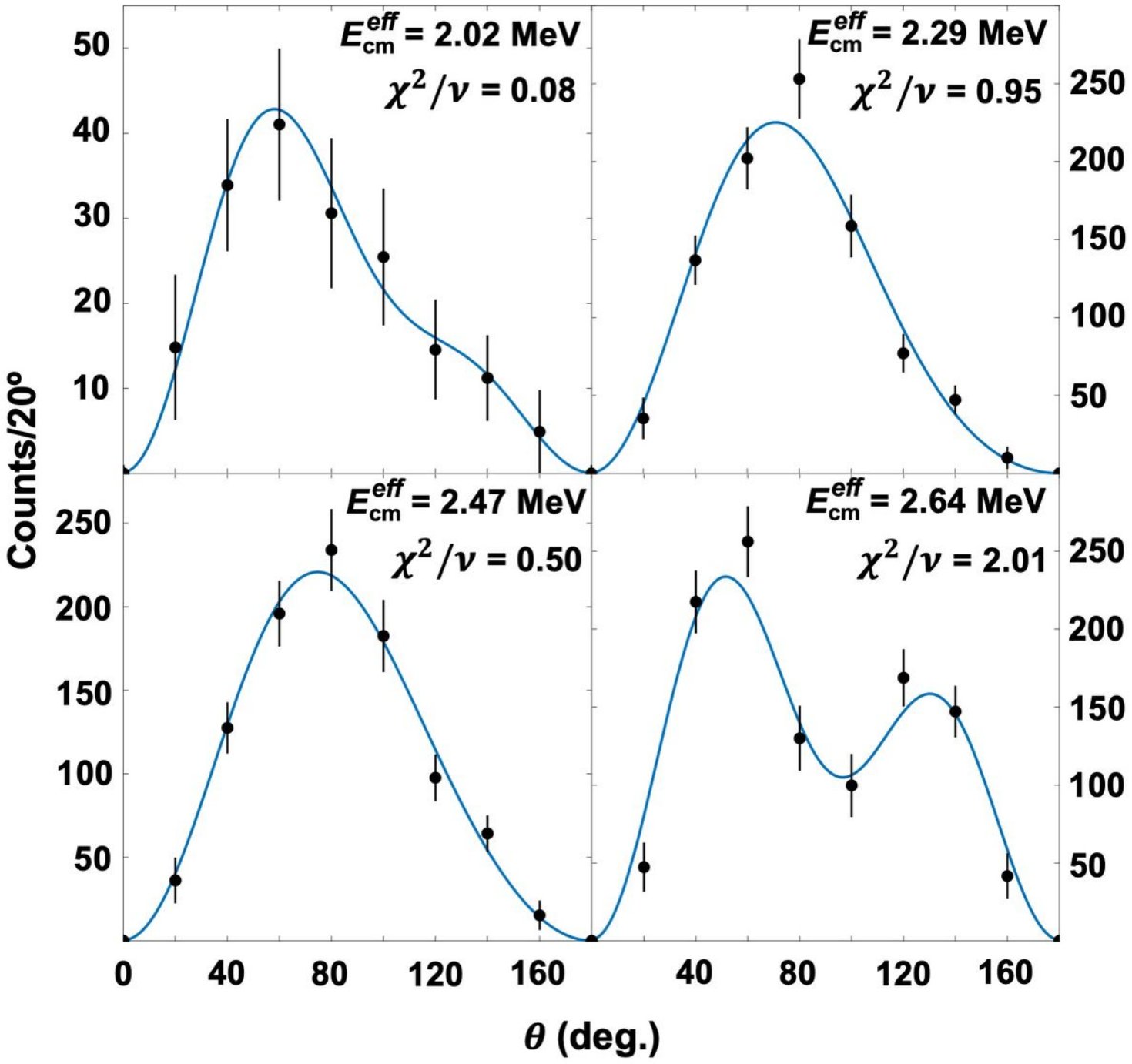

Figure 4

The measured angular distributions (including effciency corrections) at the shown "effective" centre of mass energies, with the three parameter fit (jAE1j, jAE2j, and 12) of the partial wave decomposition.

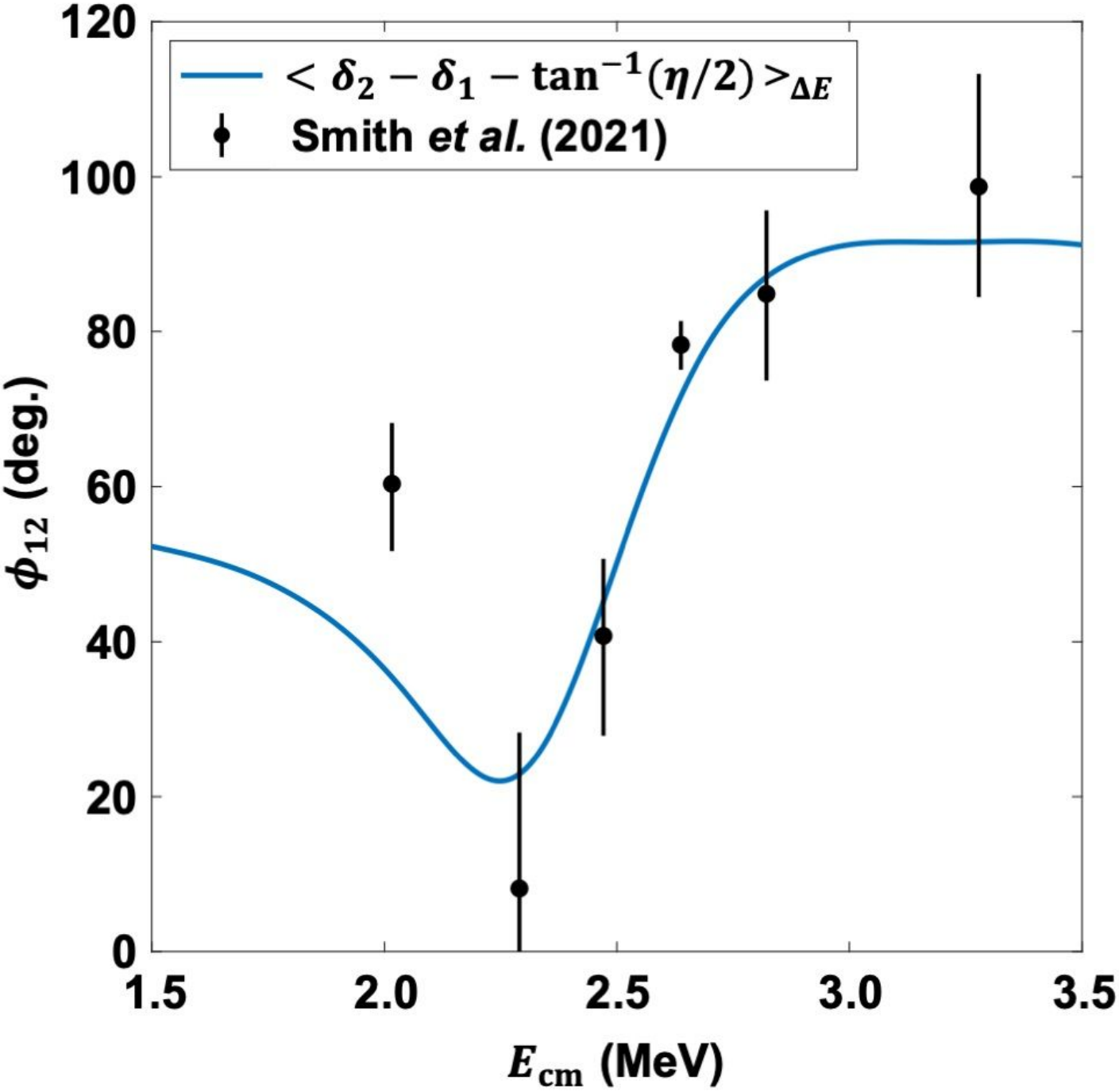

Figure 5

The measured E1-E2 mixing phase angle (o12), compared to the phase angle predicted by unitarity, convolved with the gamma beam energy resolution of a ~ 120 keV, shown as the solid line.

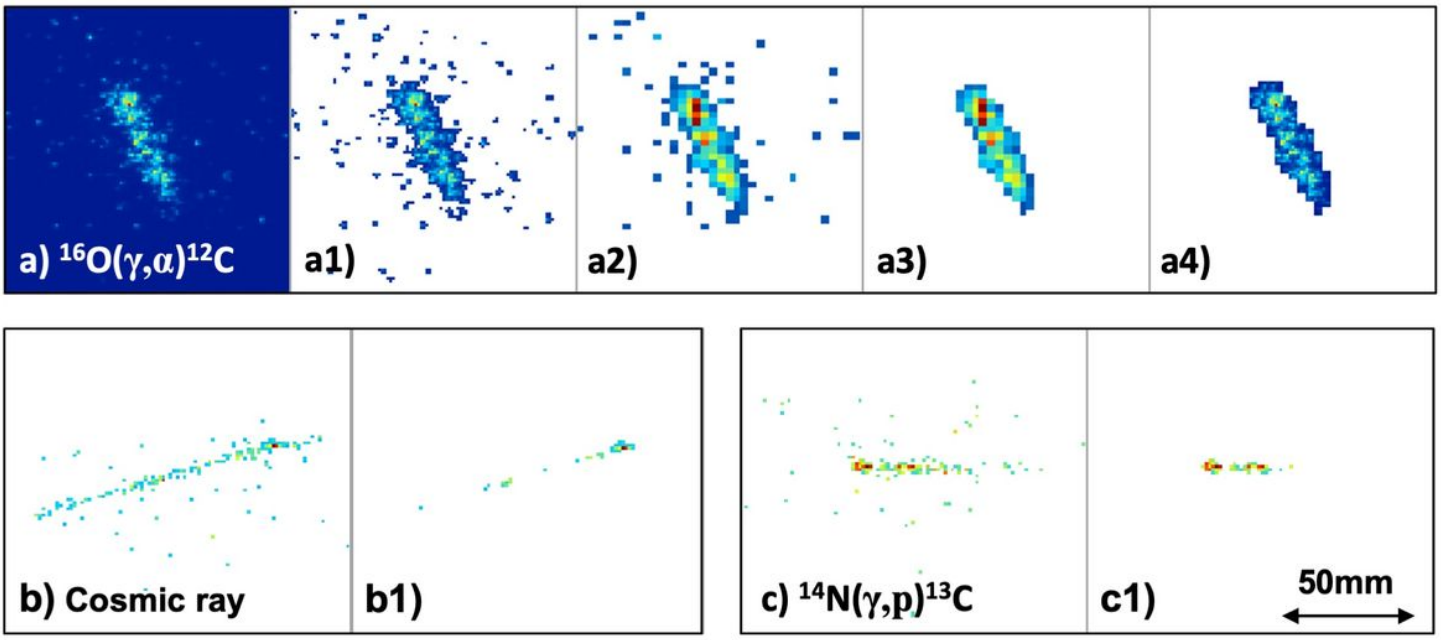

Figure 6

Image processing steps for the photo-dissociation and cosmic events: a) 16O(y , a)12C, b) cosmic ray, c) 14N(y , p)13C.

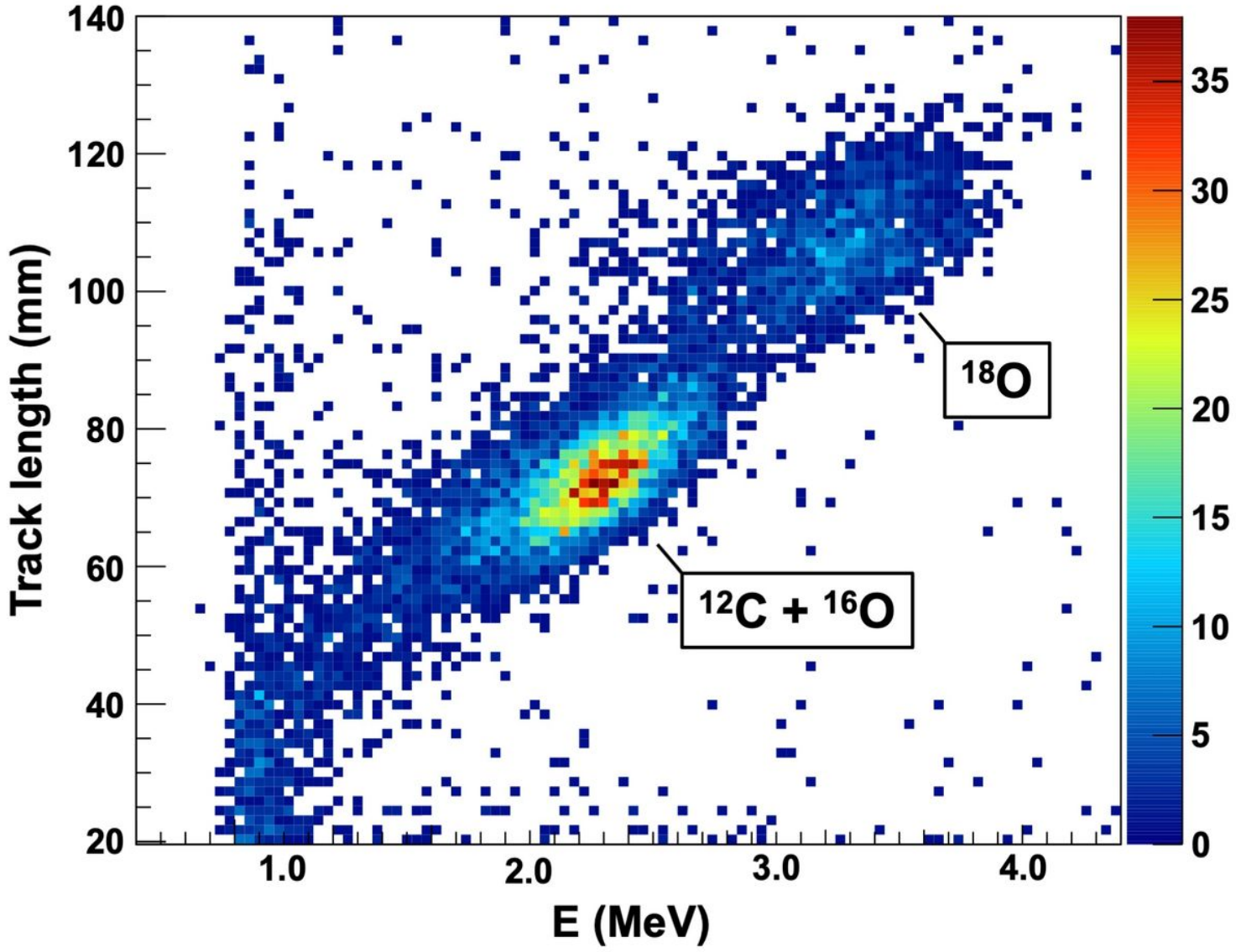

Figure 7

Histogram of track length vs. deposited energy.

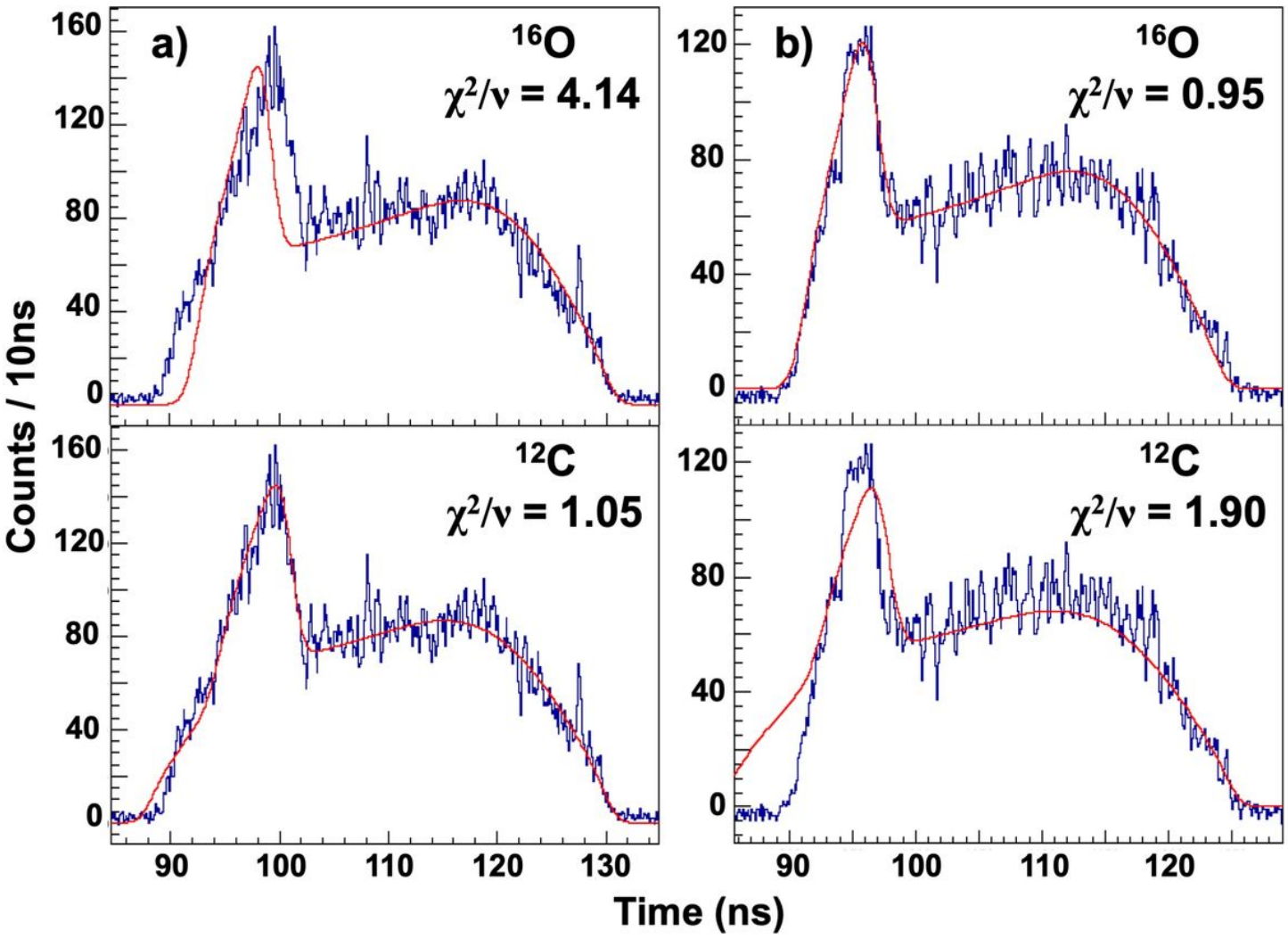

Figure 8

Example lineshape fits used to distinguish 12C/16O events. a) A typical 12C photo-dissociation time projection. b) A typical 16O photo-dissociation time projection. The upper and lower panels show the best fits of 16O and 12C photo-dissociation theoretical lineshapes, respectively.